Title: Dendritic spikes expand the range of well-tolerated population noise structures

Alon Poleg-Polsky

Department of Physiology and Biophysics, University of Colorado School of Medicine, Aurora, CO 80045, USA. alon.poleg-polsky@ucdenver.edu

Abstract:

The brain operates surprisingly well despite the noisy nature of individual neurons. The central mechanism for noise mitigation in the nervous system is thought to involve averaging over multiple noise-corrupted inputs. Subsequently, there has been considerable interest recently to identify noise structures that can be averaged out to preserve reliable signal encoding. By analyzing realistic synaptic integration in biophysically accurate neuronal models, I report a role for a complementary de-noising approach mediated by focal dendritic spikes. Dendritic spikes might seem unlikely candidates for noise reduction due to their miniscule integration compartments and poor averaging abilities. Nonetheless, the extra thresholding step introduced by dendritic spike generation could increase neuronal tolerance for a broad category of noise structures, some of which cannot be resolved well with averaging. Computations with multiple dendritic spikes compensate for compartment size constraints and expand the repertoire of conditions that can be reliably processed by neuronal populations.

Introduction

Neurons generate variable responses to the repetitive presentation of the same stimulus (Faisal et al., 2008). This variability, or noise, can corrupt the neuronal representation of the signal and limit the amount of usable information in neuronal populations (Kohn et al., 2016). Numerous

models have examined the function of neural networks in noisy conditions (Faisal et al., 2008; Franke et al., 2016; Kohn et al., 2016; Zylberberg et al., 2016; Zylberberg et al., 2017). In virtually all studies, neurons were formulated to integrate their synaptic inputs linearly (McCulloch and Pitts, 1990). However, most biological neurons are not linear integrators of synaptic inputs. Instead, neurons have internal computational compartments formed by dendritic spikes (Branco and Hausser, 2010; London and Hausser, 2005; Major et al., 2013; Schiller et al., 2000; Spencer and Kandel, 1961). Coordinated synaptic activation, clustered on a small region of an individual branch (Major et al., 2008; Schiller et al., 2000) can recruit dendritic voltage-gated channels and N-methyl-D-aspartate receptors (NMDARs). Sufficiently strong activation of these channels leads to a positive feedback loop forming the regenerative dendritic spike. The resulting amplification of the synaptic drive to the dendrite could potentially function to boost representation of salient input patterns (Hawkins and Ahmad, 2016; Lavzin et al., 2012; Palmer et al., 2014; Schmidt-Hieber et al., 2017; Smith et al., 2013).

The size of the dendritic integration compartment and the somatic depolarization following dendritic spike generation depend on cell type, and the location of the stimulated region (Branco and Hausser, 2011; Major et al., 2008), and can be surprisingly small. Often, activation of just a handful of synaptic inputs is sufficient for dendritic spike generation (Branco and Hausser, 2011; Major et al., 2008; Schmidt-Hieber et al., 2017). Small integrative compartment sizes and limited interactions with synaptic inputs elsewhere on the dendritic tree (Poirazi et al., 2003; Polsky et al., 2004) form the backbone of independent dendritic computational units (Hausser and Mel, 2003; Hawkins and Ahmad, 2016; Rhodes, 2008; Wu and Mel, 2009). Dendritic subunits can theoretically substantially increase neuronal abilities to process and store information; yet, small

dendritic compartment sizes may pose a challenge for informative computations in the presence of a noisy synaptic drive.

To illustrate the idea, consider the case of a neuron tasked with discriminating between two stimuli. We assume that the cell is innervated by a presynaptic population of neurons that change their firing rate depending on signal identity. In this example, the presence of the preferred stimulus is encoded with 1 AU firing rate and a null (distractor) stimulus with 0.5 AU (Figure 1 A). We now ask how active synaptic integration of these inputs affects the ability of the postsynaptic cell to differentiate between the stimuli.

In the absence of noise, linear integration of the presynaptic inputs results in two perfectly separatable postsynaptic signals (Figure 1 A, E dotted lines). A linear integrator can perform this task even in the presence of significant input variability. For example, a stochastic process with Poisson-like (variance=mean, see methods) variability, a noise structure that is common in the brain (Smith et al., 2013; Zhu et al., 2015; Zylberberg et al., 2016), significantly affects signaling intensities in individual presynaptic cells (Figure 1 B). However, linear integration of multiple presynaptic inputs reduces the trial-to-trial variability of the postsynaptic signal (the postsynaptic variability is proportional to the presynaptic variability divided by the square root of the number of inputs, Figure 1 B, right, E). Linear synaptic integration appears therefore to be an appropriate mechanism to preserve the separation between postsynaptic stimuli representation in the presence of stochastic noise (Figure 1 G, red).

In contrast to the whole-cell linear integrator, similar noise structures degrade the reliably of synaptic integration in dendritic subunits (Figure 1 H). As dendritic spikes sample only a tiny

portion of the total synaptic drive to the cell, integration of synaptic inputs in the presence of stochastic noise is associated with high postsynaptic trial-to-trial variability (Figure 1 I). This variability lessens the accuracy of input amplification by dendritic spikes (Figure 1 J), producing false positive (amplification of the weak stimulus) and false negative (a lack amplification of the strong stimulus) responses (Fig 1 J, black). This result suggests that synaptic integration in a dendritic compartment is unreliable in the presence of stochastic noise, indicating a potential computational weakness of dendritic subunits (Figure 1 M, red).

In this study, I examine whether the enlistment of active dendritic subunits affects the robustness of neuronal computations in noisy environments. By analyzing postsynaptic responses to different population activity patterns, I propose a novel role for dendritic spike threshold as a powerful denoising mechanism. Interestingly, my results indicate that dendritic subunits are exceptionally capable of mitigating noise structures that are resistant to averaging, such as stimuli misclassification. Accordingly, the integration of misclassified synaptic inputs improves significantly in neuronal models that incorporate active dendrites. Furthermore, I show that information processing in parallel dendritic subunits is tolerant to various presynaptic noise structures. Taken together, the processing abilities of dendritic spikes challenge the noise tolerance rules formulated for linearly integrating neurons and extend the dynamic range of biological brains.

Results

The simple model shown in Figure 1 suggests that stochastic variability has a high potential to have a negative impact on the performance of dendritic subunits. This observation does not

mean that nonlinear dendritic computations require low-noise operating conditions. Instead, dendritic spikes may not be particularly well suited to resolve high-variance noises. Considering that recent physiological and modeling studies support the assumption that stochastic noise is not the only and likely even not the most prevalent noise structure in the brain (Babadi and Sompolinsky, 2014; Beck et al., 2012; Gollnick et al., 2016), it may be relevant to explore synaptic integration in dendrites in the presence of other presynaptic noise structures.

Dendritic spikes can theoretically enhance postsynaptic responses to classification errors

As an inspiration for a non-trivial noise source, I have considered synthetic digital systems. A common communication error in computers is a (mis)classification error, also known as a bit encoding error, which manifests as a mismatch between the transmitted and the received signals (Shannon, 1948). On Figure 1 C I examined the effect of classification errors on signal decoding in the simple neuronal model. Unlike stochastic noise that changed the amplitude of the presynaptic responses, classification errors affected the consistency of stimuli encoding. In the noise-free condition, the higher/lower firing rates always corresponded to the preferred/null stimuli respectively. In the presence of classification errors, some of the presynaptic cells were simulated to respond with 1 AU to null and 0.5 AU to preferred stimuli (Figure 1 C, F). In the presented example, I randomly flipped signal encoding in this way in 15% of the inputs. These stimulus encoding errors affect the ability of the postsynaptic cell to determine stimulus identity because of the decreased difference between postsynaptic stimuli representations (Figure 1 F). In our case, the analytical solution for the mean summed signal is

$$\Sigma\omega_1=[x_1\cdot(1-E_r)+ x_2\cdot E_r]\cdot n$$

107 Where $\Sigma\omega_1$ is the summed input to stimulus 1 in the postsynaptic cell, x_1 and x_2 are the noise-
108 free responses in individual presynaptic cells to the two stimuli (1 and 0.5 AU), E_r is the error rate
109 (15%), and n is the number of presynaptic inputs. As follows from the equation, classification
110 errors would always affect the mean postsynaptic response, and the difference between the
111 postsynaptic signals should diminish proportionally to the imposed error rate (Figure 1 F, G,
112 blue).

113 Additionally, in contrast to stochastic noise, pooling across large presynaptic pool does not
114 reduce the negative impact of classification errors. Therefore, averaging is not a viable strategy
115 to address misclassification. Instead, this input structure necessitates a denoising mechanism
116 that is based on a decision threshold – such as the threshold formed by regenerative dendritic
117 spikes. In fact, a handful of synaptic inputs are sufficient for a threshold-based mechanism to
118 establish reliable (with >95% accuracy) responses (Figure 1 K-M). As I show below in multi-
119 compartmental neuronal models performing biologically relevant computations, realistically
120 formulated dendritic compartments can categorize stimuli accurately in the presence of
121 classification errors. Moreover, dendritic spikes dramatically improve neuronal robustness to
122 noise and sharpen signal representations in neural networks, unlike linearly integrating cells.

123 *Comparison between integration schemes in a multi-compartmental model*

124 Motivated by the predictions of the simple model, I set out to probe signal processing in a
125 detailed multi-compartmental NEURON model of a layer 2/3 cortical pyramidal cell (see
126 methods). I considered an innervation scenario where stimulus identity set the number of spikes
127 in the presynaptic cell population (Figure 2, methods). The temporal sequences of the

128 presynaptic firing patterns were generated semi-randomly in each simulation run (Figure 2,
129 methods). To approximate a linear synaptic integration, I distributed the α-amino-3-hydroxy-5-
130 methyl-4-isoxazolepropionic acid receptor (AMPAR)-containing synapses randomly over the
131 entire dendritic tree of the postsynaptic cell (Figure 2 A, B). AMPAR conductance is ohmic;
132 henceforth this integration model will be referred to as 'ohmic-linear'. To model synaptic
133 integration with dendritic computational units, I clustered a group of synapses containing both
134 AMPAR and NMDARs on a single dendrite to facilitate generation of NMDA spikes (Figure 2 C, D).

135 The postsynaptic cell could discriminate between the stimuli in both integration modes (Figure 2;
136 Figure 2-figure supplement 1). To draw informative comparisons between integration schemes, I
137 gradually increased the number of synaptic inputs in the dendritic spike integration scenario
138 until the number of somatic spikes matched the postsynaptic output of the ohmic-linear model
139 (2±0.1 APs, Figure 2-figure supplement 1). Stimulation of eight clustered synaptic inputs reliably
140 invoked dendritic spikes and matched the somatic firing rate obtained with 200 AMPAR-only
141 synapses for the preferred stimulus (Figures 2, 2-figure supplement 1).

142 *Distinct noise tolerance of dendritic spikes is evident in a multi-compartmental model*

143 I found presynaptic noise structures to have characteristic effects on the integration of synaptic
144 information. The stochastic noise did not significantly affect the mean number of postsynaptic
145 spikes recorded in the ohmic-linear integration scenario (Figure 3-figure supplement 1 A, B, left).
146 To quantify the ability of the postsynaptic cell to differentiate between the stimuli, I used the
147 Receiver Operating Characteristic (ROC) curve, a commonly used discrimination metric to
148 examine the true positive as a function of the false positive rates at various threshold settings.

149 The normalized area under the ROC curve can vary between 0.5 - no discrimination and 1 -
150 perfect performance. The area under the ROC curve measured for the postsynaptic firing was
151 not affected by the introduction of the stochastically variable synaptic drive (from 0.9±0.05 in
152 control to 0.92±0.06 with noise, Figure 3 A, left). In line with the prediction of the simple model,
153 this noise structure had a pronounced effect on postsynaptic signaling in dendritic
154 computational subunits, mainly due to an elevated rate of false negative responses, were
155 preferred stimulation was not followed with a postsynaptic AP (Figure 3-figure supplement 1 A,
156 B, right). Consequently, the area under the ROC curve was reduced from 0.99±0.01 in control
157 conditions to 0.78±0.07 in the presence of stochastic presynaptic synaptic drive (Figure 3 A,
158 right).

159 Similar results were observed when the information content of the postsynaptic output was
160 measured with a mutual information metric (methods). The peak information in a binary
161 discrimination task is 1 bit per trial, and a random input conveys zero bits. In the ohmic-linear
162 model, the stochastic noise did not change the postsynaptic information rate (Figure 3 B, left). As
163 discrimination was nearly perfect for synaptic processing with dendritic subunits in control, the
164 information was close to unity (0.99±0.01 bits), and dramatically diminished in the presence of
165 stochastic input variability the (0.37±0.09 bits, Figure 3 B, right; $p<0.001$, $n=1000$, ANOVA
166 followed with Tukey test).

167 Next, I repeated the simulations in the presence of classification errors. In the ohmic-linear
168 integration scenario, classification errors reduced the difference between the number of somatic
169 spikes evoked by the two stimuli - despite signal transformation by somatic threshold
170 nonlinearity (Figure 3 A, left). Subsequently, the area under the ROC curve and mutual

171 information calculated from the postsynaptic firing were significantly degraded by classification
172 errors (Figure 3 A, B, left). In contrast to the ohmic-linear scenario, the effects of classification
173 errors on synaptic integration with dendritic spikes were quite mild. Both the area under the
174 ROC curve (0.92±0.05, Figure 3 A, right) and the postsynaptic mutual information (0.75±0.08,
175 Figures 3 B, right, 3-figure supplement 2, right) improved over the simulations in the presence of
176 stochastic noise. These results, observed over a wide range of synaptic inputs to the dendritic
177 computational unit (Figure 2-figure supplement 1) and error rates (Figure 3-figure supplement
178 1), echo the enhanced tolerance of dendritic compartments to misclassification errors seen in
179 the simple model (Figure 1).

180 To control for the possibility that the difference between synaptic integration scenarios
181 originated due to a different postsynaptic glutamate receptor composition, I examined synaptic
182 integration with voltage-independent (ohmic) NMDARs (Figure 3-figure supplement 3, methods).
183 Ohmic NMDARs preserved the prolonged postsynaptic depolarization observed in dendritic
184 subunits but did not evoke dendritic spikes (Figure 3-figure supplement 3). Due to the loss of
185 dendritic amplification, a comparable number of synapses were required to induce somatic firing
186 either when inputs were clustered on an individual branch or randomly distributed over the
187 whole cell. Unlike in control conditions, however, the information capacity of dendritic synaptic
188 integration with ohmic NMDARs was reduced in the presence of classification errors (Figure 3-
189 figure supplement 3). The result mirrors globally distributed ohmic-linear integration (Figure 3, 3-
190 figure supplement 3) and implies that generation of dendritic spikes mediates the tolerance of
191 dendritic subunits to classification errors.

192 *Enhanced robustness of dendritic computation of direction selectivity to classification errors*

In the simulations presented above, the computational task was binary discrimination between stimuli. In the following section I examined whether the effects of noise on postsynaptic computations can be generalized to direction selectivity (DS), a classic neuro-computation commonly used to analyze neuronal responses in the presence of noise (Cafaro and Rieke, 2010; Franke et al., 2016; Kohn et al., 2016; Zylberberg et al., 2016). Direction selectivity and the related computation of orientation selectivity often recruit dendritic computational subunits (Lavzin et al., 2012; Oesch et al., 2005; Sivyer and Williams, 2013; Smith et al., 2013; Trenholm et al., 2014; Wilson et al., 2016) and thus represent relevant computational task to compare between linear and dendritic subunits integration models.

I probed direction selectivity by recording the firing in the postsynaptic cell in response to directional cues coming from the synaptic drive. In brief, directional tuning of each presynaptic cell set its firing rate. For consistency with previous simulations, the tuning curve of the cell peaked at its preferred direction (PD) and elicited twice as many presynaptic spikes as did the null direction (ND) (Figure 4 A, black). The amplitude and the direction of the preferred response varied between presynaptic cells (methods).

The stochastic noise was modeled as before (Figure 4-figure supplement 1). To account for multiple directions of stimulation, I implemented classification errors by shifting the directional preference of presynaptic cells (Figures 4 B, 4-figure supplement 1). In each simulation trial, I rotated the entire directional tuning curve for each presynaptic cell by a random value taken from a normal distribution with a standard deviation of 45° (Poleg-Polsky et al., 2018). This effect mirrors labile directional tuning found experimentally in the cortex (Benucci et al., 2013; Felsen et al., 2002; Jeyabalaratnam et al., 2013) and other brain regions (Rivlin-Etzion et al., 2012).

215 Next, I recorded dendritic potentials and somatic signals in the presence of stochastic noise
216 (Figure 4 C, D) and classification errors (Figure 4 E, F). I first examined the sharpness of
217 directional tuning with Direction Selectivity Index ($DSI = \frac{PD-ND}{PD+ND}$). The tolerance of direction
218 selectivity computation to presynaptic variability was generally similar to the two-stimulus
219 discrimination task described above.

220 In the ohmic-linear integration, the DSI of the postsynaptic cell was only marginally better in
221 noise-free simulation than the DSI of the input (0.39±0.32 vs. 0.33, Figures 4 G, left, 4-figure
222 supplement 1). Direction selectivity improved with stochastic noise to DSI=0.51±0.37 and
223 became reduced with classification errors (0.25±0.23, Figure 4 G, left; $p<0.001$ between the
224 three simulated conditions, n=1000, ANOVA followed by Tukey test). Similar trends were
225 observed for the information content of the postsynaptic cell (Figures 4 G, right, 4-figure
226 supplement 1) and the variability of the computed angle of the postsynaptic PD (Figures 4 H, 4-
227 figure supplement 1, methods).

228 In the active dendritic integration scenario, noise-free stimulation at the ND seldom provoked
229 dendritic spikes - resulting in an excellent postsynaptic DSI and high information content
230 (0.84±0.22 and 1.2±0.02 bits/trial respectively, Figures 4 I, black, 4-figure supplement 1). As seen
231 above for the binary discrimination task, the computation was significantly impacted by the
232 presence of stochastic noise (Figure 4 I, J, red), but less so by classification errors (Figures 4 I, J,
233 blue, 4-figure supplement 1).

234 *Dendritic computations in the presence of background synaptic activity*

235 In the simulations presented so far, the postsynaptic cell was stimulated with signal-bearing
236 synapses only. However, cortical cells in-vivo are exposed to a seemingly random background
237 synaptic bombardment (London et al., 2010; Petersen, 2017). Variable membrane potentials
238 mediated by the background drive can directly affect dendritic spike generation (Lavzin et al.,
239 2012; Major et al., 2008; Smith et al., 2013). Can dendritic computations remain reliable in this
240 challenging condition?

241 To assess the sensitivity of dendritic processing to a more realistic synaptic environment, I added
242 a signal-independent synaptic background. This background activity consisted of excitatory and
243 inhibitory synapses distributed randomly over the dendritic tree (Figure 5 A, C, methods).
244 Activation of these inputs depolarized the cell, increased the trial-to-trial variability of the resting
245 membrane potential and introduced background firing (Figure 5 B, D) (Fellous et al., 2003). The
246 modeled cell was able to discriminate between preferred and null stimuli across background
247 bombardment levels and integration scenarios. Both in the ohmic-linear and in active dendritic
248 models postsynaptic firing gradually increased as a function of background activity intensity
249 (Figure 5 E, F, left). Because both preferred and null responses were elevated by the same
250 amount, the information content of the neuronal output was preserved for a most tested
251 background bombardment levels (Figure 5 E, F, right). As before, dendritic computations in the
252 presence of classification errors consistently outperformed stochastic noise simulations, while
253 the opposing trend was observed in the ohmic-linear integration scheme (Figure 5 E, F, right).

254 *Dendritic spikes enhance noise tolerance of neural networks*

255 The difference between the suboptimal transformation of directional information in a realistic
256 neuronal morphology to the linear expectations from conceptual neuronal models could have
257 significant implications for signal processing in neuronal populations. Do the effects of
258 noise/errors on the propagation of information between processing layers abide by the logic
259 described for synaptic integration in a single cell or perhaps by a different set of rules, as
260 suggested recently (Zylberberg et al., 2017)?

261 To examine this question, I implemented a 2-layered feed-forward network of multi-
262 compartmental neurons. Neurons in the first network layer (L1) were innervated exclusively with
263 the signal bearing inputs, as in Figures 2-3, without background bias. Neurons in the second layer
264 (L2) combined the output of multiple L1 cells (Figure 6, methods). The simulation was executed
265 for various combinations of a different number of inputs to L1 cells and network sizes.

266 Processing in a network composed of ohmic-linear processing cells generally improved signal
267 discrimination(Figure 6 B-D). However, this was not universally the case; Figure 6 C, bottom
268 shows the mean mutual information obtained from L2 cells innervated either by 200 (solid) or
269 400 (dotted) L1 cells. Whereas integration of 200 L1 cells produces almost perfect discrimination
270 (black, measured as information rate of 1 bit per trial), the information in a network composed
271 of 400 L1 cells is not significantly different from discrimination in typical L1 neuron (Figure 6 B,
272 bottom).

273 If filtering of synaptic input by two threshold nonlinearities underlies the beneficial effect
274 observed in dendritic spike simulations, a 2-layered ohmic-linear cell network should improve
275 stimulus discrimination in the presence of classification errors. At odds with this assumption,

276 however, the mutual information computed from the output of a network of ohmic-linear cells
277 (Figure 6 C, D, blue) was often significantly below the level of signal discrimination observed in a
278 cell with active dendritic subunits (Figures 3; 6, F, blue).

279 In agreement with the unique role of dendritic spikes in synaptic processing, a network
280 consisting of neurons with nonlinear dendritic subunits consistently enhanced signaling across
281 processing layers (Figure 6 E-H). In most simulations, L2 cells did not fire spikes to the null
282 stimulus (Figure 6 G, top). The improvement in mutual information was especially prominent for
283 stochastic noise (Figure 6 G-H, red) and signal discrimination was perfect for many network
284 arrangements in the absence of noise or with classification errors (Figure 6 G, H). These results
285 promote the view that signal-processing abilities of a single cell with dendritic computational
286 units can outperform signal manipulation in a network composed of multiple ohmic-linear
287 neurons. Furthermore, as a network of neurons with dendritic computational subunits can
288 compensate for the low stochastic noise tolerance observed at the level of a single cell (Figure 3,
289 red), dendritic processing in a neural network increases the robustness of neuronal
290 computations to a wide range of input conditions.

291 *Enhanced noise tolerance in a neuron with multiple dendritic computational subunits*

292 Having established the ability of a neural network to withstand stochastic noise, I set out to
293 examine whether similar noise tolerance can take place within a single neuron. Synaptic
294 information flow in large pyramidal cells conceptually follows the architecture of a 2-layered
295 network (Poirazi et al., 2003; Polsky et al., 2004). In this formulation, individual branches form a
296 dendritic processing layer that sums synaptic inputs up to dendritic spike threshold. The output

297 from the dendritic computation compartments combines at the soma, forming the second
298 computational layer.

299 In contrast to previous simulations, where all signal-bearing synapses targeted a single branch, in
300 my next model I distributed 30 synaptic inputs over five basal dendrites of a cortical layer 5
301 pyramidal cell (Figure 7 A, see Figure 7-figure supplement 1 for integration over a different
302 number of inputs). The choice of the neuron is justified: dendritic spikes generated on the distal
303 portion of the basal dendrites of layer 5 cells are typically subthreshold to somatic AP, and a
304 cooperative activation of multiple dendritic units is required to reach somatic threshold (Figure 7
305 A, inset) (Major et al., 2008; Polsky et al., 2009; Polsky et al., 2004). In the simulated layer 5 cell,
306 postsynaptic firing was likely with two or more dendritic spikes and spikes in four or five
307 dendritic compartments essentially guaranteed a supra-threshold somatic response (Figure 7 A).

308 Synaptic integration with multiple dendritic subunits in control conditions and with classification
309 errors was comparable to the performance of a cell with a single dendritic compartment (Figures
310 3, 7 C, D). A pronounced positive effect of multi-compartmental integration was observed in the
311 presence of stochastic noise, where the information present in the postsynaptic output, while
312 still lower than in noise-free condition (Figure 7 D; 0.79±0.05 vs. 0.98±0.05, $p<0.001$, $n=1000$,
313 ANOVA followed by Tukey test), dramatically improved compared to the single dendritic spike
314 case (Figure 3).

315 Finally, careful inspection of the findings suggested that the enhanced noise tolerance found in a
316 layer 5 cell could be due to the increased overall number of activated synapses. If the number of
317 inputs sets the noise tolerance rules, stochastic noise may perform equally well in a layer 5

318 neuron with a single dendritic compartment. Conveniently, both the size of the dendritic
319 computation unit - in terms of a the number of inputs required to generate a dendritic spike -
320 and the resulting peak somatic depolarization increase for proximal stimulation locations
321 (Behabadi et al., 2012; Major et al., 2008). I found that focal stimulation with 30 inputs at a spot
322 located 45 µm from the soma drives AP generation with metrics that are similar to multi-
323 dendrite simulation in control (noise-free) condition (Figures 7 E-H, 7-figure supplement 1,
324 black). The postsynaptic response profile in the presence of stochastic noise and classification
325 errors in the single proximal stimulation scenario was indistinguishable from the multi-dendrite
326 simulation (Figure 7 red, blue). This result supports the conclusion that the more substantial
327 number of inputs required to trigger somatic firing in layer 5 pyramidal cells could assure
328 robustness to noise.

329 Discussion

330 Here I describe for the first time that neuronal computations with dendritic processing units do
331 not follow the noise tolerance rules established in conventional population models. Simple
332 considerations and biophysically realistic neuronal models demonstrate different denoising
333 strategies and robustness to dissimilar noise structures between linearly integrating neurons and
334 synaptic input transformation with dendritic spikes (Figure 8).

335 In mammals, various neuronal types possess the necessary dendritic machinery for focal
336 dendritic spike generation (Manita et al., 2017). Dendritic spikes are potent mediators of somatic
337 firing (Grienberger et al., 2014; Oesch et al., 2005; Palmer et al., 2014; Schmidt-Hieber et al.,
338 2017). They contribute to neuronal computations in-vivo and correlate with perception (Lavzin

339 et al., 2012; Manita et al., 2017; Schmidt-Hieber et al., 2017; Smith et al., 2013; Takahashi et al.,
340 2016; Wilson et al., 2016). The calcium influx associated with a dendritic spike is an important
341 mechanism for induction of synaptic plasticity (Gambino et al., 2014), linking dendritic
342 regenerativity with learning (Kaifosh and Losonczy, 2016; Schiess et al., 2016) and memory
343 formation (Guerguiev et al., 2017; Sheffield and Dombeck, 2015). These multiple lines of
344 investigation strongly suggest that reliable dendritic spike generation is essential for brain
345 function.

346 *Integration of different noise sources*

347 Currently, the consensus is that by combining neural responses, the brain can then average out
348 the impact of noise and increase the signal to noise ratio (SNR). Averaging is especially useful in
349 limiting stochastic fluctuations in synaptic signals – implying that stochastic noise is relatively
350 benign for a linear synaptic integration, but only when the sampled presynaptic population is
351 large. As I show here, due to their relatively small integrative compartment seizes, dendritic
352 spikes could be particularly sensitive to stochastic synaptic signal variability at the SNR levels that
353 are present in the brain (Magee, 2000; Smith et al., 2013; Zavitz et al., 2017; Zylberberg et al.,
354 2016). This disruptive potential of stochastic noise can be partially negated by at least three
355 strategies as revealed in this work: larger dendritic compartment size (Figure 7), synaptic
356 integration in multiple dendritic subunits on the same neuron (Figure 7), or in subunits across
357 different cells (Figure 6).

358 While most studies on neural computations to date assumed a stochastic population noise
359 structure, noise representation in the brain is a fundamental open question in neuroscience. I

take the question of 'what is noise?' one step further. A broad class of neuronal computations can be formulated as discrimination problems, where the network is tasked with sorting the input into distinct categories. Beck et al (2012) provided compelling theoretical evidence to suggest that misclassification noise is practically unavoidable in complex nervous systems due to suboptimal inference (Beck et al., 2012). Misclassifications plague artificial neural networks; our conscious experience suggests that classification errors are common in biological brains. Instead of treating classification errors as computational failures, I propose to consider them as a noise source that decreases the accuracy of the computation. Despite the high trial-to-trial SNR levels in the presence of classification errors, linear mechanisms cannot average away this noise, irrespective of the size of the presynaptic population (Figures 1, 3) and the number of neurons dedicated to the task (Figure 6). Critically, the situation is different with active dendritic computations. Nonlinear dendritic synaptic integration utilizes spike threshold to increase the reliability of presynaptic input classification (Figures 1, 3). In Figures 1-3, I showed how this process works for a binary decision process; the probability of dendritic spike initiation encodes the information in the case of a continuous variable (Figure 4). These results are consistent and expand previous theoretical observations that dendritic computations are reliable with high SNR input manipulations (Hawkins and Ahmad, 2016; Rhodes, 2008; Wu and Mel, 2009).

Evidence for classification noise in neurons

Experimental results support the notion that classification errors are present in the brain. Cortical responses to sensory stimulation can be binary, composed of a single or no action potentials, as originally described by DeWeese et al. in the primary auditory cortex of the rat (DeWeese et al., 2003) and more recently seen in a mouse barrel cortex (Hires et al., 2015;

382 Ranjbar-Slamloo and Arabzadeh, 2017). Neurons in these areas fire for most, but not all,
383 repeated stimulation trials and often have a non-zero background firing rate in the absence of
384 stimulation (DeWeese et al., 2003; Tao et al., 2016). This response profile is incompatible with a
385 Poisson process (DeWeese et al., 2003). Instead, these responses are identical to the binary
386 classification errors described here (Figures 1, 3).

387 Classification errors are harder to distinguish from the stochastic process for a stronger firing
388 response (DeWeese et al., 2003; Tao et al., 2016) and more complex stimulation paradigms
389 (Poleg-Polsky et al., 2018). A useful criterion that can discriminate between different noise
390 structures is symmetry. By definition, stochastic process elicits responses that are normally
391 (symmetrically) distributed around the noise-free mean (Poleg-Polsky et al., 2018). Thus, trial-to-
392 trial response variability that is not symmetric is likely to arise from a different source. An
393 example of a complex, non-stochastic signal variability in the brain was demonstrated by Gollnick
394 et al. (Gollnick et al., 2016). The authors revealed a probabilistic cortical population encoding of
395 whisker deflection intensity where the sensory input affected the likelihood of a neuronal
396 response, but not the mean response intensity. Furthermore, the magnitude of whisker
397 deflection could not be estimated correctly with a linearly operating ideal observer, in line with
398 my findings that linear decoders fail with a non-stochastic input profile.

399 *Active dendrites and neural networks*

400 The presented evidence points to the conclusion that the common assumption that ohmic-linear
401 synaptic integration with AMPARs is similar to an idealized linear integrator is incorrect.
402 Especially telling was the observation that a network composed of ohmic-linear cells

403 underperformed as a binary discriminator, as in many cases it did not fare better than a single
404 ohmic-linear cell, while neurons with dendritic amplification mechanism excelled in this task
405 (Figure 6). This finding resonates with progressive enhancement of metrics of direction and
406 orientation selectivity in the cortex. In mice, thalamic input to V1 is weakly tuned (Sun et al.,
407 2016) similar to the presynaptic drive used in current simulations (Figure 4). The increase in
408 cortical visual selectivity between processing layers is most pronounced in neurons that exhibit
409 dendritic nonlinear input-output transformation (Wilson et al., 2016), [but see (Jia et al., 2010)].
410 Suppression of dendritic spikes in the cortex by hyperpolarization or intracellular perfusion of
411 NMDAR blockers decrease subthreshold and suprathreshold selectivity, confirming that dendritic
412 amplification mechanisms are crucial for synaptic integration (Lavzin et al., 2012; Smith et al.,
413 2013). With newly emerging imaging technologies, it will be possible to probe the dendritic
414 input-output signal transformation experimentally and to gain a deeper understanding of the
415 mechanistic basis of processing of sensory information in the brain.

416 To conclude, I argue that while computations with dendritic spikes are necessary to enhance
417 biologically relevant signal features, noise tolerance of dendritic processing units is tuned to
418 noise structures that differ from the 'benign' noise types established for linearly integrating
419 neurons (Figure 8). The degree by which population noise interferes with neuronal computations
420 should, therefore, be studied in the context of postsynaptic integration. These conclusions are
421 based on analysis of a binary discrimination task and direction selectivity, but they should
422 generalize to many neuronal computations and apply to a range of tasks solved by our brains.

423 Acknowledgments

I thank Gautam Awatramani, Jeffrey Diamond and Joel Zylberberg for helpful comments on the manuscript.

Methods

The simulations were conducted on multicompartmental models using the NEURON 7.4 simulation platform. The modeled cells were subdivided into 483-1022 compartments, with a maximum length of 19 µm. For the layer 2/3 pyramidal cell, the area of the soma was 1350 μm^2, and the total dendritic length was 3320 μm^2. For layer 5 pyramidal cell, somatic area was 2380 μm^2, and the total dendritic length was 9420 μm^2. The resting membrane potential was set to -60 mV, the membrane resistance was set to 10,000 $\Omega \cdot cm^2$, the axial resistance was 100 $\Omega \cdot cm$, and the membrane capacitance was set to 1 $\mu F/\mu m^2$. The simulations that included sodium and potassium voltage-gated currents used Hodgkin-Huxley kinetics formalism. Specifically, fast sodium channels (reversal potential=50 mV, gNa=200 mS/cm^2), and delayed rectifier and slow non-inactivating potassium channels (reversal potential=-87 mV, gKdr=30 mS/cm^2 , gKs=1 mS/cm^2) were used to allow for spike generation and adaptation, respectively (Lavzin et al., 2012).

Synapses: Excitatory postsynaptic synapses contained AMPARs and NMDARs. AMPAR currents had an instantaneous rise time and a decay time of 1.5 ms. NMDAR currents had a rise time of 2 ms and a decay time of 100 ms. The synaptic current reversed at zero, and the unitary AMPAR/NMDAR conductance was 1 nS. The NMDAR conductance voltage dependence was modeled as follows: $gNMDA=\frac{1}{1+0.25e^{-0.08Vm}}$ where Vm is the local membrane potential. When ohmic-linear synaptic integration was modeled, synapses were distributed over the entire

445 dendritic tree and NMDAR conductance was typically set to zero to prevent spurious dendritic
446 spike generation by randomly clustered synapses. When indicated, voltage-independent
447 NMDARs were included ohmic-linear distribution. In these simulations, the voltage factor in
448 NMDAR conductance was set to the resting membrane potential (-60 mV) for the duration of the
449 simulation. In simulations with inhibitory $GABA_A$ synapses, GABAergic synaptic conductance was
450 set to 1 nS, the reversal potential to -70 mV, and the decay time to 7 ms.

451 Presynaptic stimulation: Directionally selective simulations: The angle of preferred direction for
452 the presynaptic cell population was chosen from a normal distribution with a mean at 180° and
453 SD of 45°. The postsynaptic cell was assumed to prefer inputs from cells aligned with its PD
454 (180°); towards this goal, the amplitude of each presynaptic cell was multiplied by $e^{-i\theta_i^2/45^2}$,
455 where θi is the difference (in degrees) between the PD angle of the presynaptic and the
456 postsynaptic cell *i* . DSI was calculated as $DSI = \frac{PD-ND}{PD+ND}$. The DSI of the presynaptic population
457 was set to 0.33. To measure the variability of the computed PDs from the 'true' PD that was
458 encoded by the presynaptic trains, I computed the difference between the postsynaptic PD and
459 true PD angles in each simulation round (composed of 8 symmetrically arranged directional
460 trials). The standard deviation of the resulting distribution was used to quantify the dispersion of
461 the estimated postsynaptic tuning (Poleg-Polsky et al., 2018).

462 The tuning profile of presynaptic cells was set according to the following generalized normal
463 distribution: $A_i = 0.5 + 0.5e^{(-\theta_i-\alpha)^4/\omega^4}$, where *Ai* is the amplitude of presynaptic cell *i*, α is the
464 angle of stimulus direction, and ω is the width of the presynaptic tuning profile (90°). Stochastic
465 noise was implemented by changing the amplitude of each presynaptic cell individually by a

466 value drawn at random for each trial from a normal distribution with the mean at 0 and variance
467 equal to the noise-free presynaptic amplitude response. In direction selective model
468 classification errors were modeled by drawing a value from a normal distribution with a mean of
469 0 and SD of 45 for each presynaptic cell; this value was then added to the PD of each presynaptic
470 cell and the tuning profile recalculated. This procedure effectively shifted the entire tuning
471 profile of each presynaptic cell by a random value independently across trials. To convert
472 between presynaptic response amplitude and firing rate, the amplitude of each presynaptic cell
473 was rounded to the nearest integer. This value indicated the number of presynaptic spikes from
474 that cell. The temporal pattern was set by NEURON's *negexp* function, with a mean interval
475 between spikes of 20 ms. In addition to stimulus-mediated presynaptic activity, all synapses had
476 a random firing at a rate of 4 Hz (1 Hz with Ohmic NMDARs) to emulate synaptic activation
477 observed in the cortex. Where simulated, background synapses were activated with random
478 firing pppattern, the average firing rate was 10 Hz.

479 Two stimuli discrimination: In these simulations the presynaptic population was modeled as in
480 the direction selectivity case. Only PD and ND (180° and 0° respectively) directions were probed.
481 In these simulations classification errors were introduced as in the simple model (Figure 1) by
482 randomly flipping signal identity in ~15% of the presynaptic cells. Discrimination (Figure 1) was
483 measured as the difference between the summed postsynaptic responses to preferred and null
484 input presentations in a given trial. Trials with stronger postsynaptic response to the null
485 stimulus were marked as reversed discrimination.

486 Analysis: The presence of dendritic spikes was measured as prolonged (>30 ms) depolarization
487 above -30 mV in the activated dendritic location. Mutual information was measured as the

entropy of signals across all stimulated directions minus the summed entropy of individual directions. Unless noted otherwise, all error bars represent standard deviations.

492 Figures

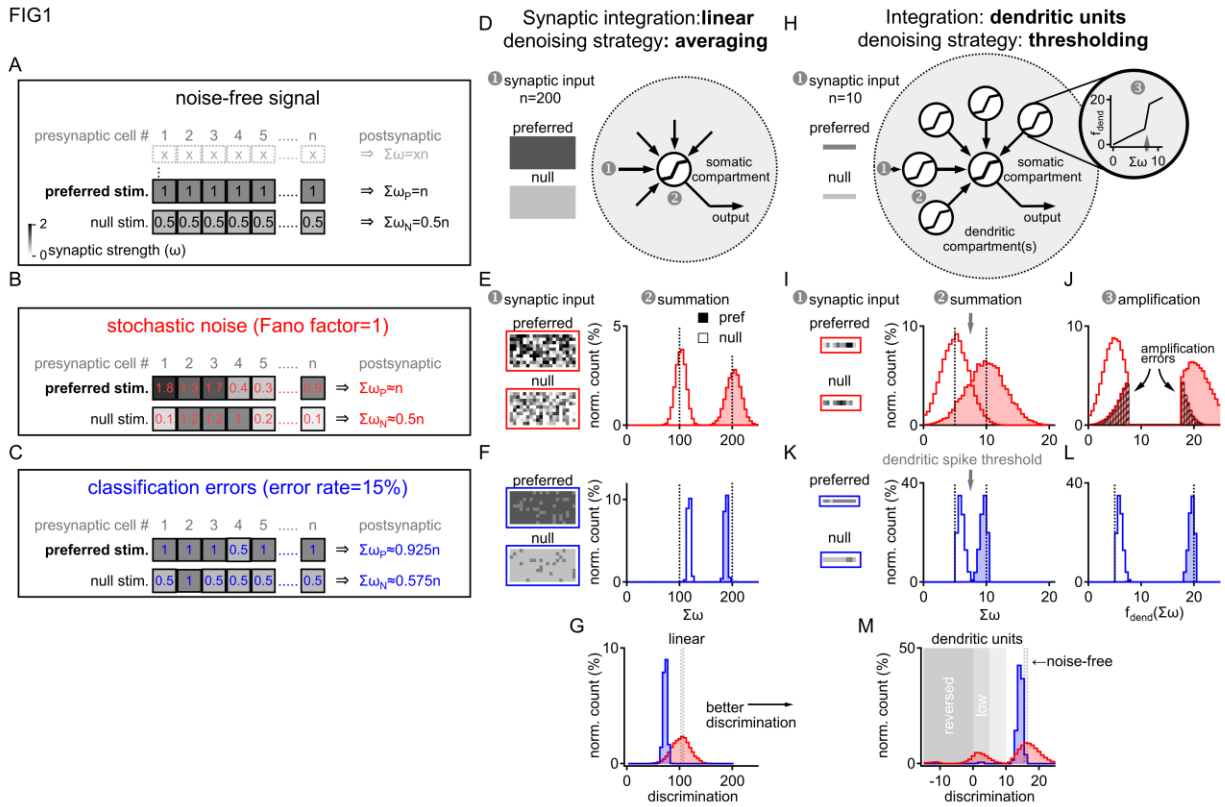

493

494 **Figure 1. Distinct denoising strategies and noise tolerance rules found in simple models of linear**

495 **and dendritic-subunit mediated synaptic integration**

496 (A) Synaptic input in the model consisted of *n* presynaptic cells; in the absence of noise, stimulus

497 intensity was identical between inputs and consisted of 1 AU for preferred and 0.5 AU for null

498 stimuli.

499 (B) Example synaptic inputs in the presence of stochastic input variability.

500 (C) Classification errors randomly flipped stimuli encoding in some presynaptic cells. Background

501 indicates input intensity.

502 (D-G) Neurons are typically assumed to combine their inputs linearly. (D, left) Example strength
503 of 200 presynaptic inputs in a single trial, color coding as in A. (E) Linear integration in the
504 presence of stochastic noise. Left, example noise-corrupted stimuli. Right, a histogram of the
505 integrated postsynaptic intensities (n=1000 trials). (F) As for (E) for classification errors. (G) The
506 difference between postsynaptic responses to preferred and null signals is maintained close to
507 noise-free levels (dotted) with stochastic noise but not in the presence of classification errors.

508 (H-M) In a more realistic integration scheme, synaptic inputs are processed first by dendritic
509 computational subunits (H). Inset, dendritic input-output transformation function. (I) As for (E)
510 for integration in a dendritic subunit. Arrow marks dendritic spike threshold. (J) Distribution of
511 postsynaptic responses following amplification with a dendritic spike. (K-L) As for (I, J) for
512 classification errors. (M) As for (G) for the output of the dendritic computational subunit.
513 Dendritic spikes accurately separated postsynaptic responses in the presence of classification
514 errors, but not in the presence of stochastic noise.

515

FIG2

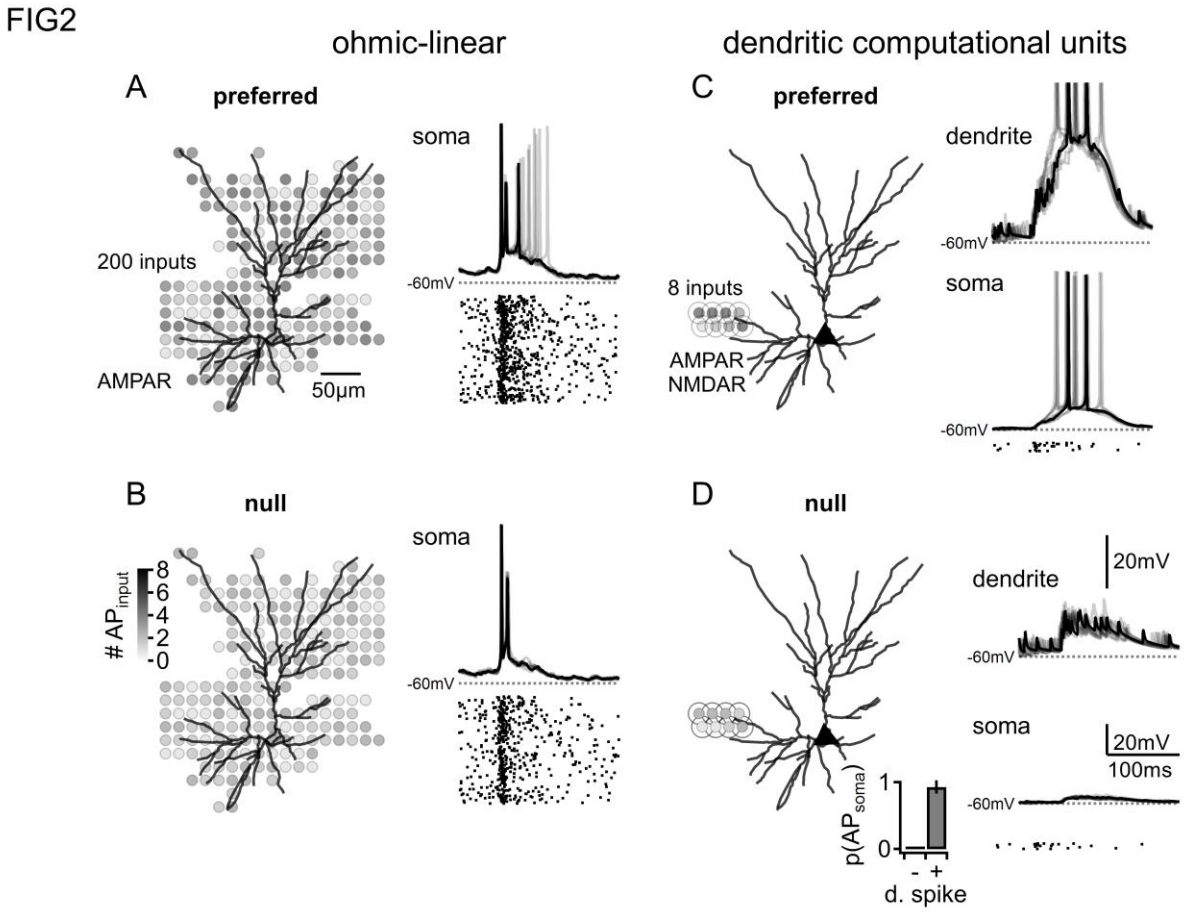

Figure 2: Synaptic integration in a reconstructed cortical layer 2/3 pyramidal cell in the absence of presynaptic noise

(A-B) Approximation of a linear integration by activation of randomly distributed AMPAR. (A) Left, synaptogram of schematic synaptic location; each synapse occupies a position on a X-Y grid near its actual location on the postsynaptic cell. Colors encode the number of stimuli-evoked presynaptic spikes in a single trial. Right, bottom, the timing of individual presynaptic spikes varied between inputs and trials. Top, the responses in the postsynaptic cell (black). Grey, postsynaptic signals in 9 similar trials. (B) As in (A) for the null signal.

526 (C-D) Dendritic computational subunits engaged by activation of clustered AMPAR/NMDAR

527 synapses. (C) As in (A) for dendritic integration with eight inputs. Top, right, responses from the

528 stimulated dendrite. (D) As in (C) for the null signal. Inset, somatic firing infallibly followed spike

529 initiation on the stimulated branch.

FIG3

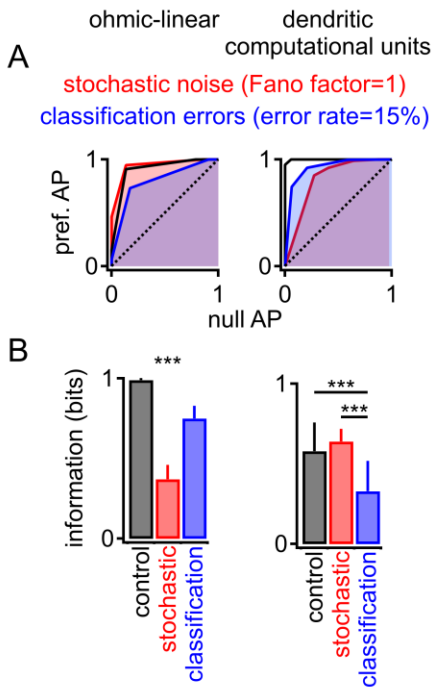

530

531 **Figure 3: Noise tolerance in a reconstructed cortical pyramidal cell**

532 (A) Receiver Operating Characteristic created by plotting the normalized number of somatic

533 spikes for the preferred stimulus vs. the normalized firing response to null stimulus presentation

534 over 1000 simulation trials. Black, noise-free simulation.

535 (B) The mutual information calculated from the postsynaptic output. Left, ohmic-linear model.

536 Right, signal processing with dendritic computational units. ***$p<0.001$, n=1000 trials, ANOVA

537 followed by Tukey test. Error bars indicate S.D.

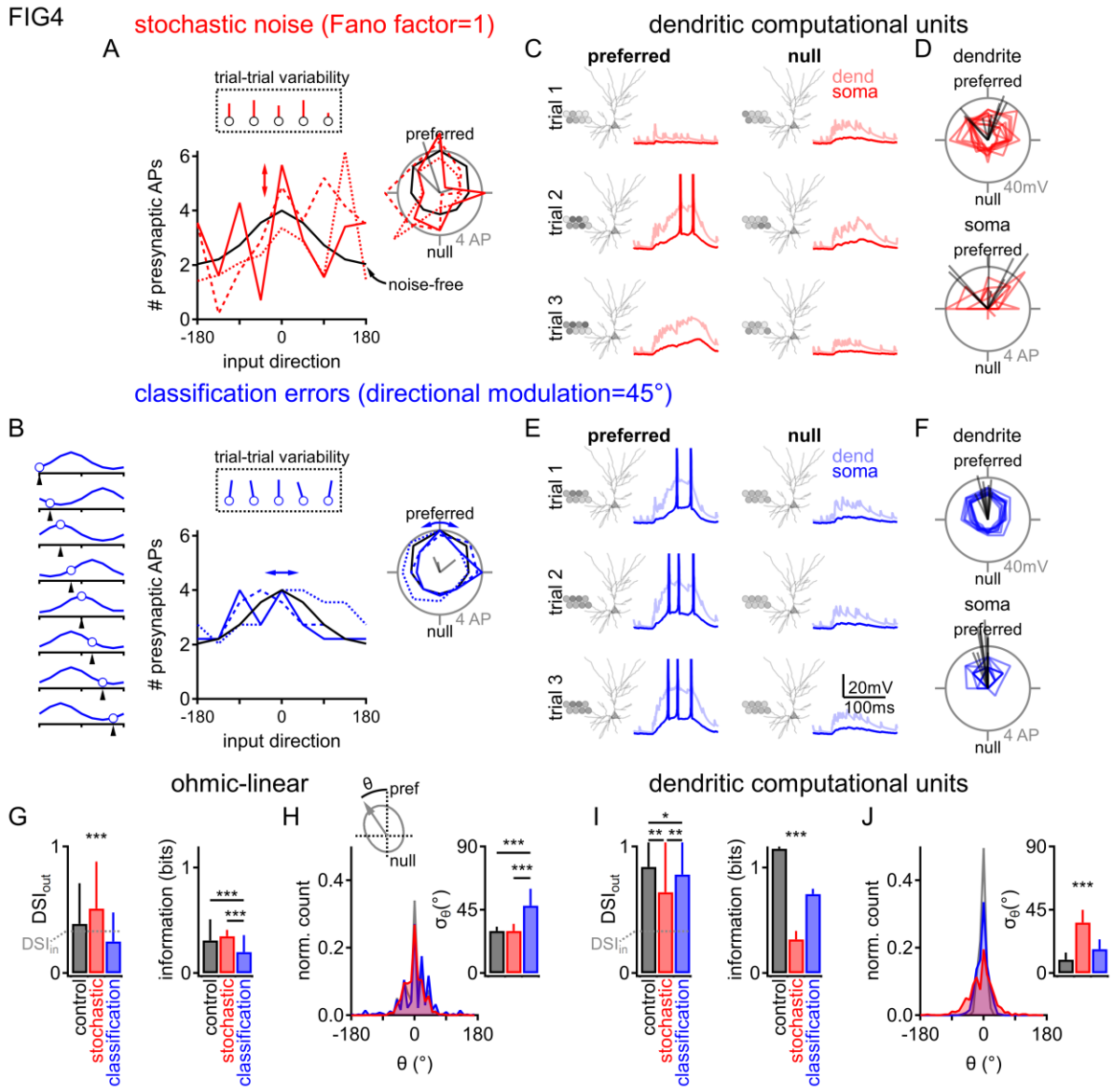

538

539 **Figure 4: The impact of noise on the computation of directions selectivity follows the rules**

540 **established in the binary classification task**

541 (A, B) Encoding of stimulus direction by noisy presynaptic population. (A) Left, example

542 directional tuning profile of a single presynaptic cell in one noise-free (black) and in three

543 stimulation rounds (one round consisted of eight symmetrically arranged directional trials) in the

544 presence of stochastic variability (red). Inset, schematic effect of the noise on presynaptic

545 stimulation intensity. Right, the same data on polar coordinates where the angle represents
546 stimulus direction and the radius represents response amplitude. Black, the vector sum of
547 individual stimulation rounds. (B) As for (A), for classification errors - shifts in the presynaptic
548 directional profile along the direction axis. Inset, classification errors ambiguate encoding of
549 signal direction. Left, example construction of a presynaptic directional curve (middle, solid blue)
550 in 8 individual trials.

551 (C-F) Synaptic integration in a dendritic subunit. (C, E) Synaptogram and voltage profiles for 3
552 example preferred (left) and null (right) stimulation trials in the presence of stochastic noise (C)
553 and classification errors (E). (D, F) Polar plots of peak dendritic EPSPs (top) and somatic spikes
554 (bottom).

555 (G) DSI (left) and mutual information (right) calculated from the somatic firing output for ohmic-
556 linear integration.

557 (H) Left, distribution of the difference (in degrees) between the PD of the input and the PD
558 calculated from postsynaptic cell. Right, the width of the distribution.

559 (I, J) As for (G, H) for dendritic subunits. *$p<0.05$, **$p<0.01$,***$p<0.001$, n=1000 rounds, ANOVA
560 followed by Tukey test. Error bars represent S.D.

561

562

FIG5

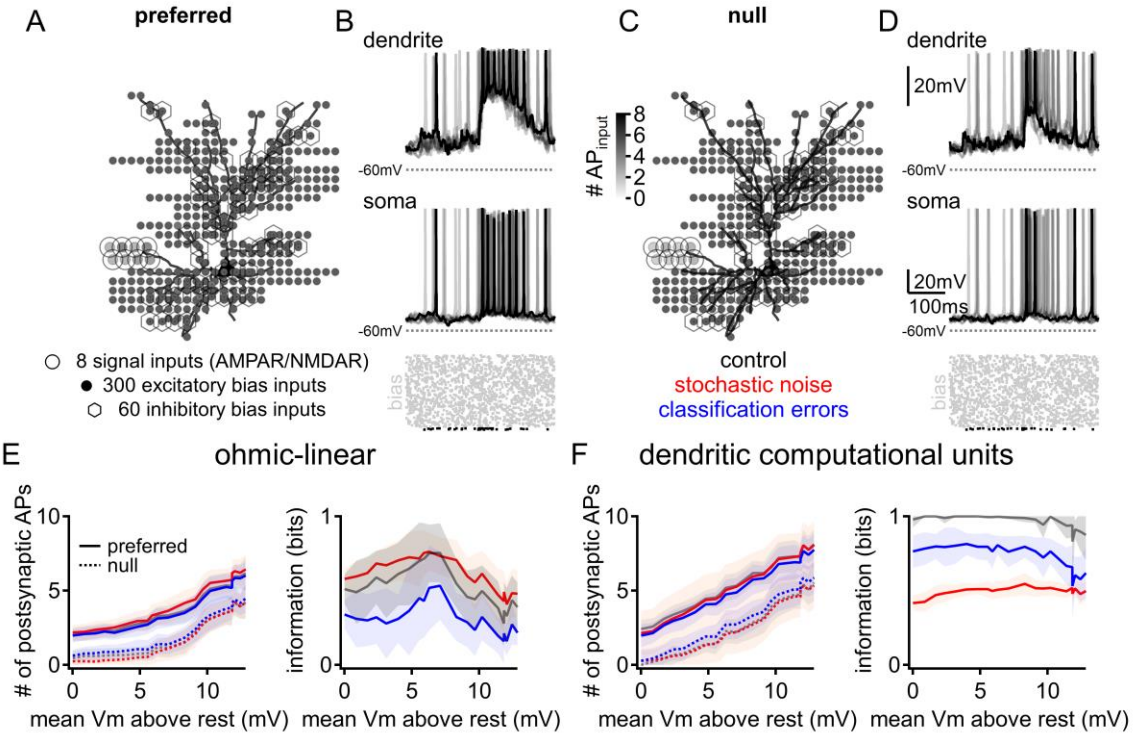

563

564 **Figure 5: A minor effect of background activity on dendritic subunits performace**

565 (A, C) Synaptogram of eight signal-mediating AMPAR/NMDAR synapses activated over a

566 background of 300 excitatory and 60 inhibitory inputs distributed randomly over the dendritic

567 tree.

568 (B, D) Bottom, the timing of the signal (black) and the background (grey) presynaptic spikes. Top,

569 the responses of the postsynaptic cell (black). Grey, postsynaptic signals in 9 similar trials.

570 (E, F) The number of somatic spikes following stimulus presentation (left) and the calculated

571 mutual information (right) as a function of the postsynaptic depolarization inflicted by

background activity in ohmic-linear (E) and dendritic computational subunits (F) models. Shades mark S.D. n=1000 repeats for each stimulus/condition.

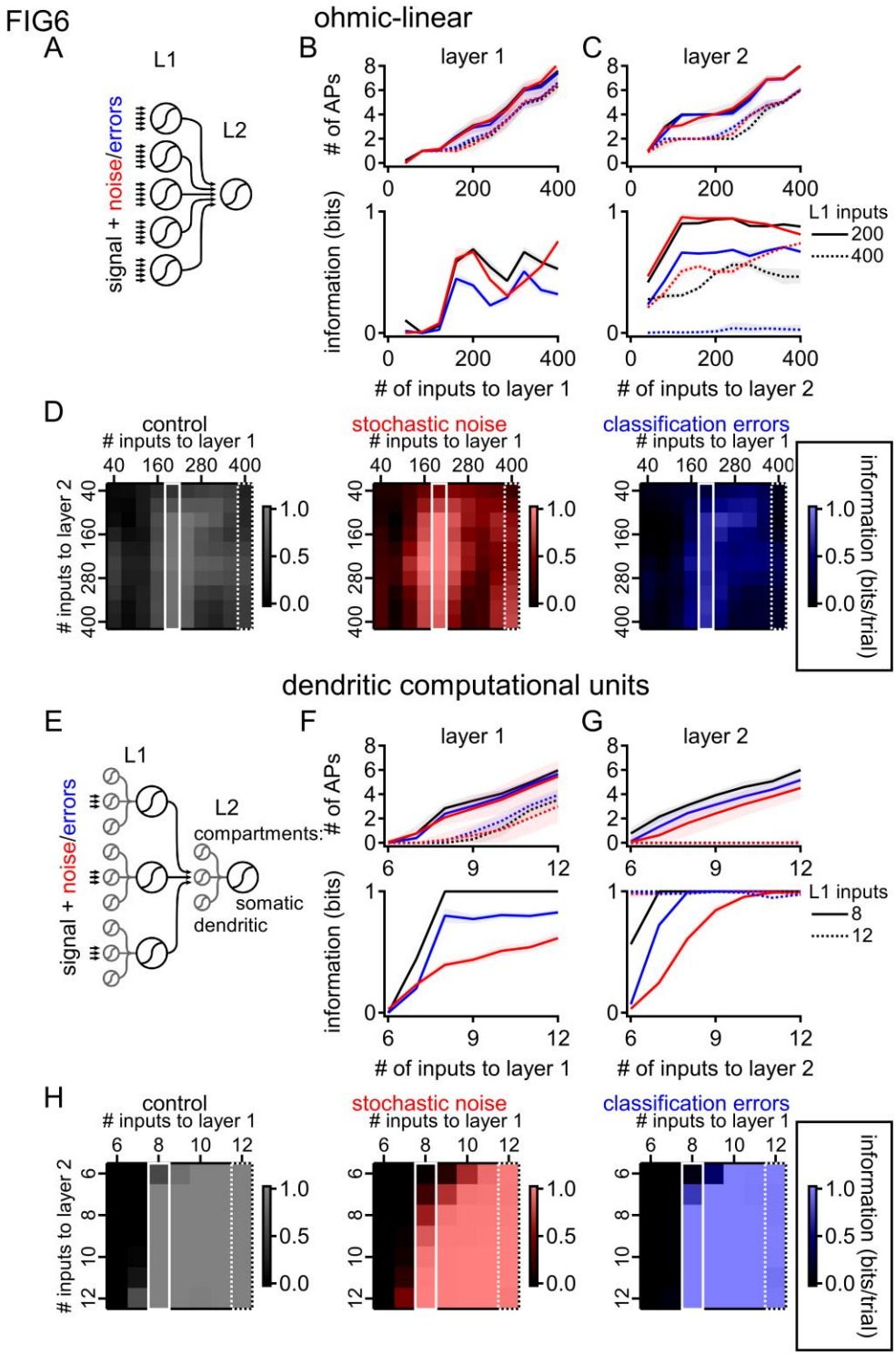

575 **Figure 6: Active dendritic integration improves processing of noisy signals in simulated neural**
576 **networks**

577 Examination of binary discrimination in a two-layered network composed of multi-
578 compartmental models of layer 2/3 pyramidal neurons with either ohmic-linear (A-D) or
579 dendritic subunit (E-H) modes of synaptic integration. Stochastic noise and classification errors
580 were implemented only at the level of the synaptic drive to the first layer (L1) cells. The firing of
581 L1 cells was used to drive synaptic activity in second-layer (L2) cells. Simulations differed by the
582 number of inputs to L1 and L2 cells.

583 (B, F) The mean number of somatic spikes (top) and the mutual information (bottom) in L1 cells
584 as a function of the number of synaptic inputs to L1.

585 (C, G) As in (B, F) for L2 cells when L1 neurons were innervated by 200 (C) or 8 (G) inputs.
586 Bottom, dotted, mutual information from L2 cells innervated with 400 (C) or 12 (G) inputs.

587 (D, H) The mean mutual information computed from L2 cells for different combinations of
588 synaptic inputs to L1 and L2 neurons (n=1000 for each configuration). Solid and dotted regions
589 indicate the network combination shown in (C, G).

590

591

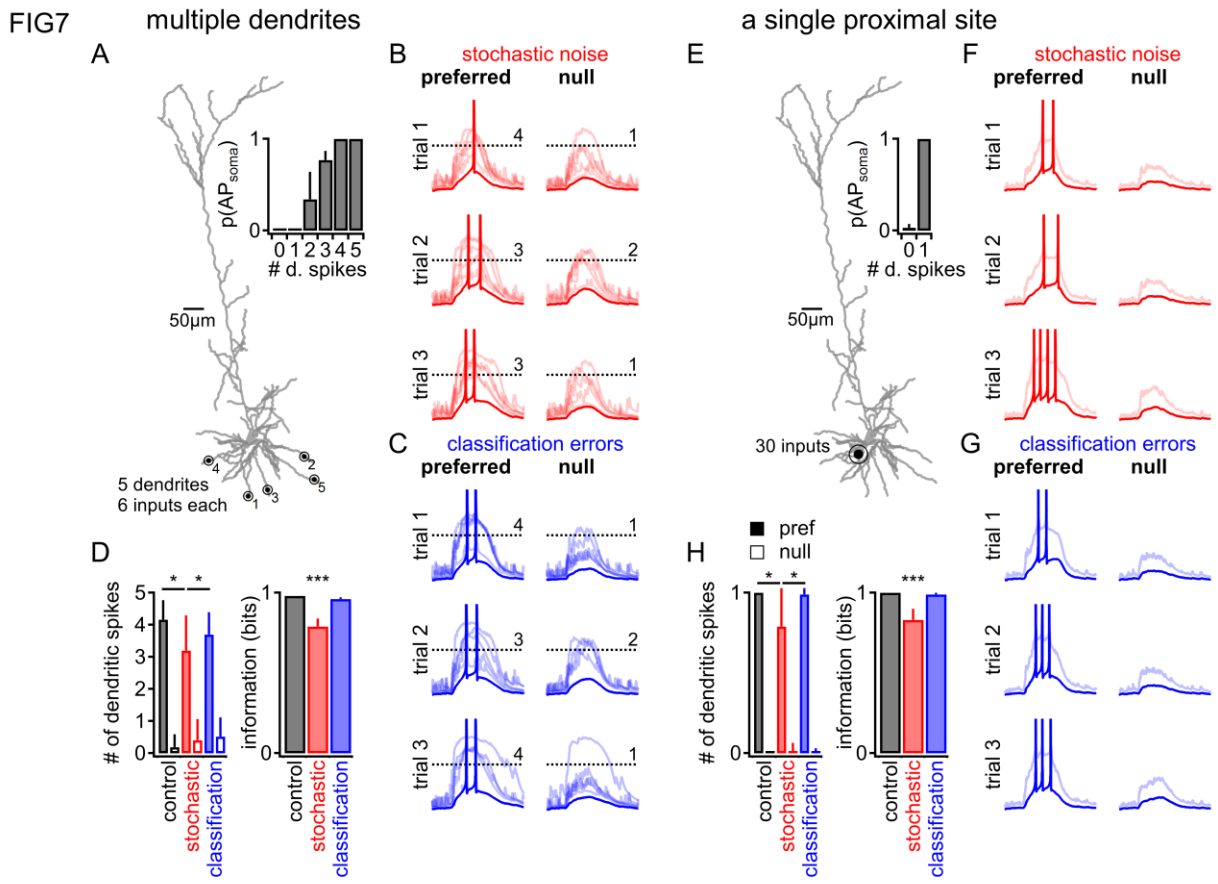

592

593 **Figure 7: The number of synaptic inputs, but not the number of dendritic processing**

594 **compartments, sets noise tolerance rules in a large pyramidal cell**

595 (A) Left, stimulation of five basal dendrites of a cortical layer 5 pyramidal cell with six

596 AMPAR/NMDAR synaptic inputs per dendrite. Right, the relationship between number of co-

597 spiking dendritic units and the probability to elicit at least one somatic action potential.

598 (B, C) Example potentials recorded at the activated dendrites (light) and at the soma (bold) in 3

599 example trials in the presence of stochastic noise (B) and classification errors (C). Noise statistics

600 as in Figure 3. The number of dendritic subunits that responded with a dendritic spike (based on

601 spike threshold crossing criteria, dotted, methods) is indicated on the right.

602 (D) The average number of dendritic spikes in preferred (solid) and null (open) stimulation trials

603 (left) and mutual information (right) estimated from 1000 simulation repeats.

604 (E-H) As for (A-D) with the same number of inputs concentrated on a single proximal spot.

605 ***$p<0.001$ vs. other conditions, ANOVA followed by Tukey test. Error bars indicate S.D.

606

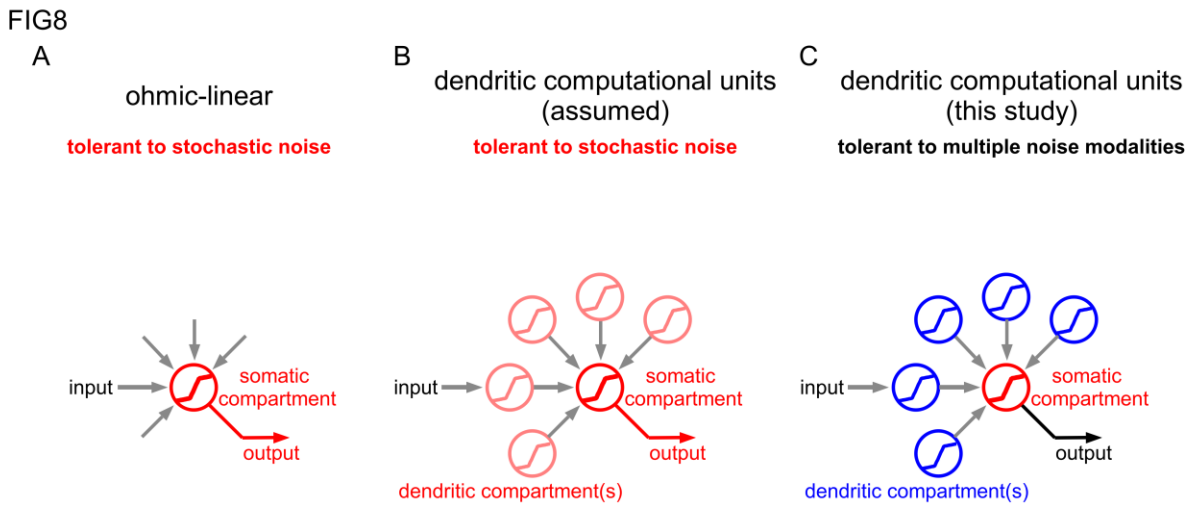

Figure 8: Summary of the main findings

(A) Traditionally, synaptic integration is considered to be linear and robust to stochastic changes in presynaptic input amplitudes (inset, red).

(B, C) Real neurons often integrate their inputs nonlinearly in dendritic computational subunits. These subunits were assumed to have a similar noise profile (B). Here I report a distinct noise tolerance of dendritic integration. While susceptible to stochastic noise, dendritic compartments excel in the presence of classification errors, a noise structure that is less optimally processed by linear mechanisms (C). Dendritic spikes can thus help to expand the repertoire of computationally benign noise structures.

619 **Supplementary figures**

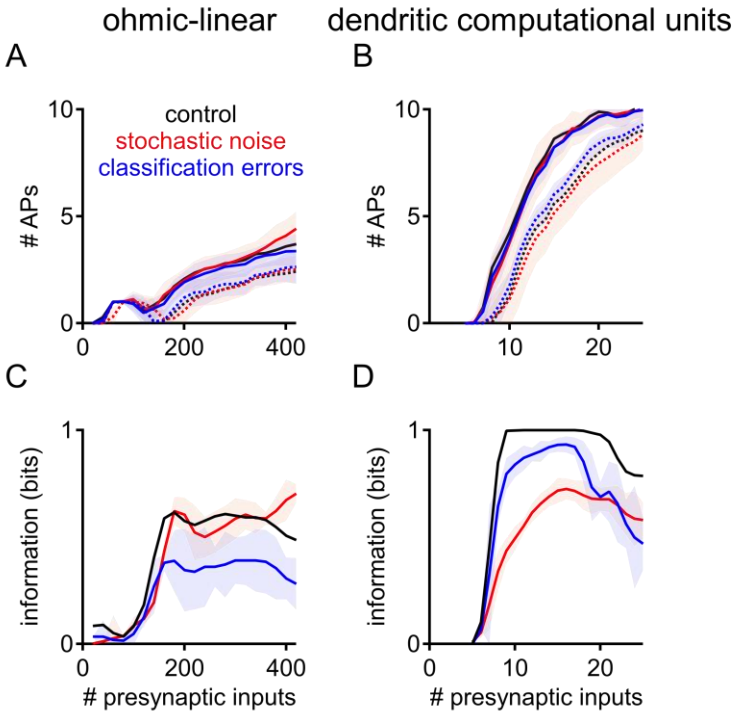

620

621 Figure 2-figure supplement 1: Postsynaptic input/output transformation in a reconstructed cortical

622 layer 2/3 pyramidal cell for a range of synaptic inputs

623 (A, C) AMPAR-only synapses, ohmic-linear integration model.

624 (B, D) Dendritic subunit integration model. (A, B) The mean number of somatic action potentials

625 for preferred (solid) and null (dotted) stimuli. Black, control (noise-free) condition. Red, with

626 stochastic input variability (Fano factor=1). Blue, in the presence of classification errors (error

627 rate=15%). (C, D) Mutual information calculated from the data in (A, B). n=1000 repeats for each

628 condition/input intensity. Shaded areas-S.D.

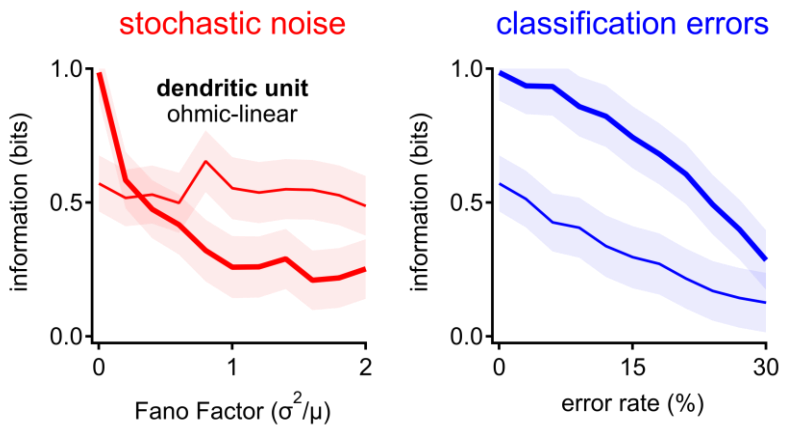

629

630 **Figure 3-figure supplement 1: Binary discrimination in a reconstructed cortical layer 2/3 pyramidal**

631 **cell as a function of noise levels**

632 Information rate per trial, measured from the number of action potentials for different

633 stochastic noise intensities (left) or classification error rates (right) in a simulated layer 2/3 cell.

634 Responses from dendritic computational subunits model (8 clustered AMPAR/NMDAR synapses)

635 are shown in bold. Thin traces indicate the linear (200 randomly distributed AMPAR-only

636 synapses) simulation scenario. Shades mark S.D.

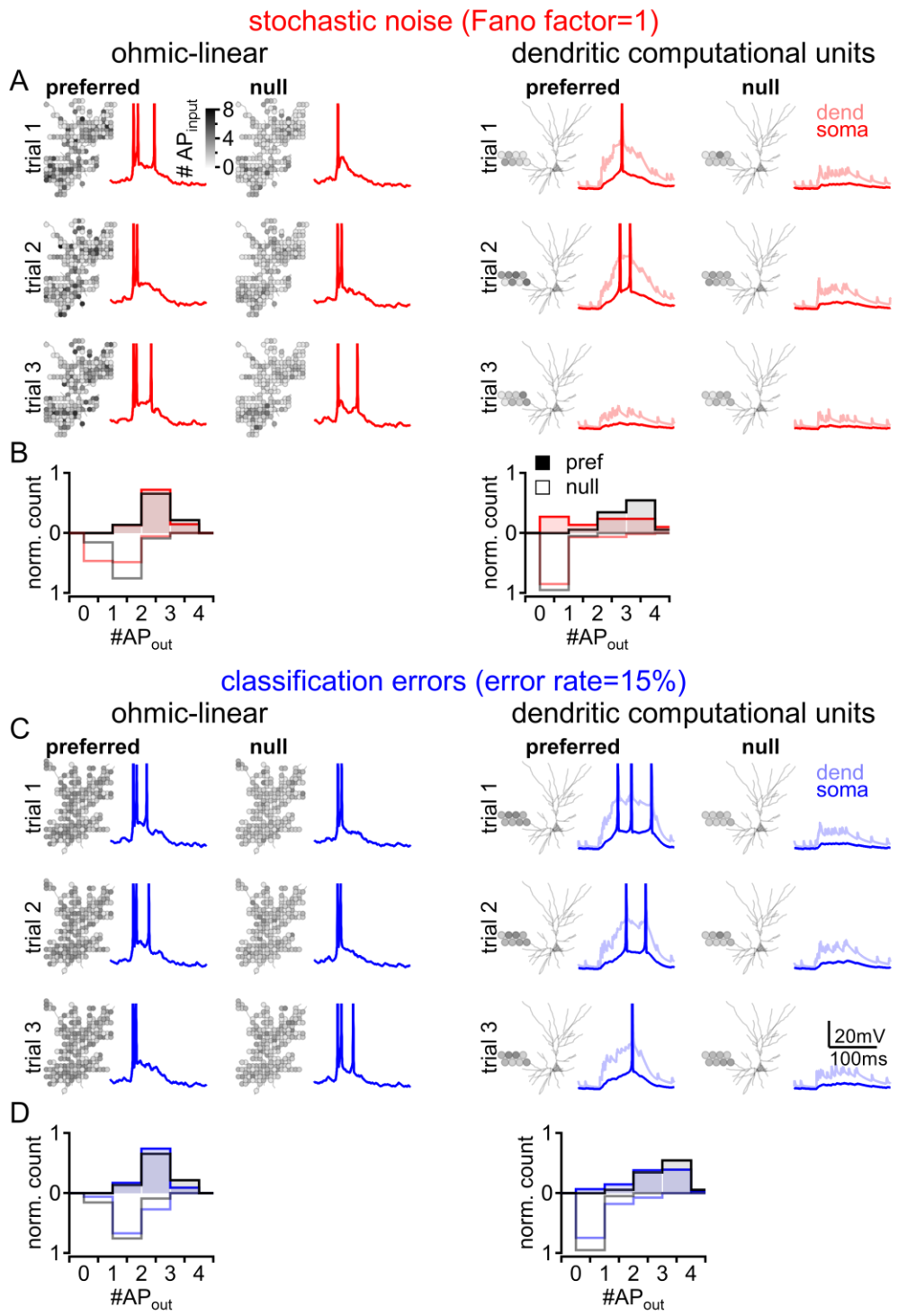

Figure 3-figure supplement 2: Examples responses in models with ohmic-linear and dendritic subunit synaptic integration modes to different noise modalities

640 Integration of 200 randomly distributed AMPAR inputs (ohmic-linear, left) or 8 clustered

641 AMPRA/NMDAR synaptic inputs (dendtiic computational units, right) in the presence of

642 stochastic noise (A, B) and classification errors (C, D). (A, C) Synaptogram (color-coded by the

643 number of presynaptic spikes) and the somatic voltage profile for 3 example preferred (left) and

644 null (right) stimulation trials. (B, D) The distribution of the number of postsynaptic spikes for the

645 two stimuli computed from 1000 simulation trials. Black, noise-free simulation.

646

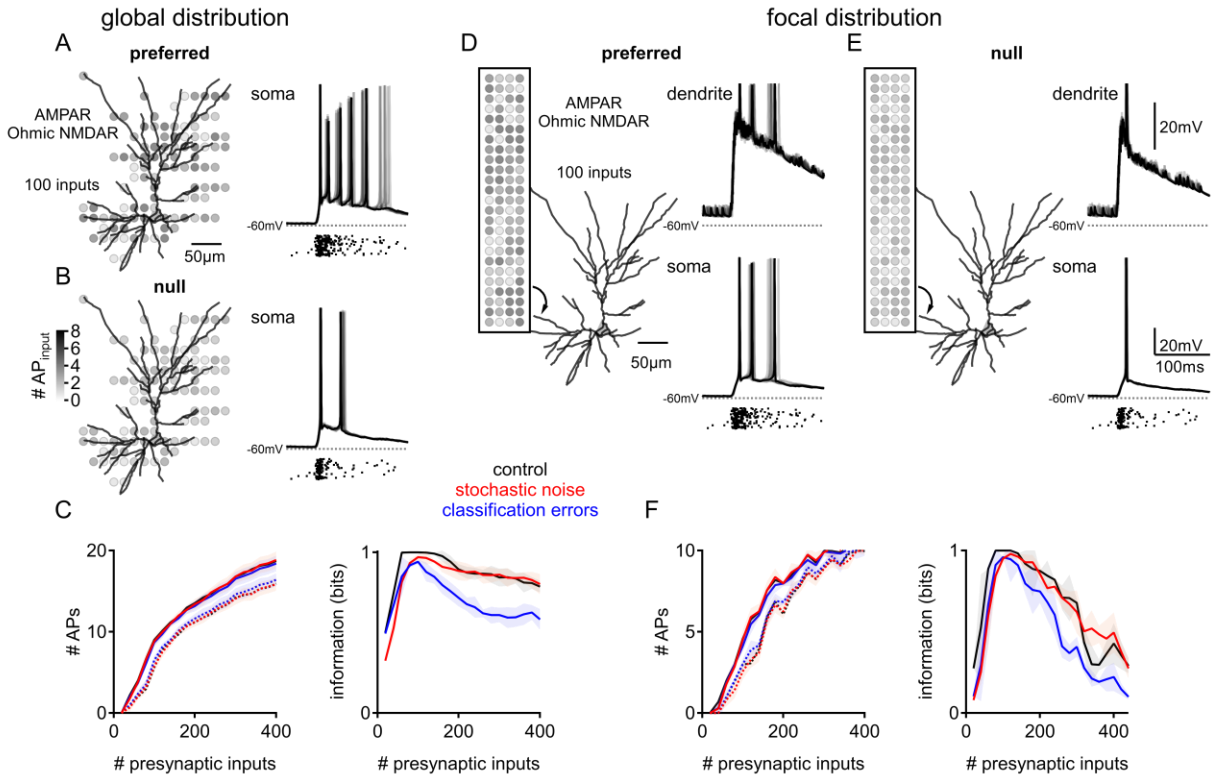

647

648 **Figure 3-figure supplement 3: Noise tolerance of synaptic integration using ohmic NMDARs.**

649 Synapses containing AMPARs and voltage-insensitive NMDARs were distrusted either randomly

650 over the entire dendritic tree (global distribution, A-C) or on were clustered on a single branch

651 (focal distribution, D-F).

652 (A) Example integration of 100 inputs activated with a preferred stimulus in noise-free condition.
653 Left, synaptogram of input intensity. Right, top, postsynaptic somatic response (black, 9
654 additional trials overlaid in grey). Bottom, the timing of presynaptic inputs activation.

655 (B) As for (A) for the null stimulus.

656 (C) Left, the mean number of somatic spikes for preferred (solid) and null (dotted) stimuli
657 presentations as a function of the number of presynaptic inputs. Right, the calculated mutual
658 information. Black, control (noise-free) condition. Red, with stochastic input variability (Fano
659 factor=1). Blue, in the presence of classification errors (error rate=15%).

660 (D, E) Integration of 100 focal synaptic inputs. Left, input location and intensity. Right, dendritic
661 (top) and somatic (middle) potentials following activation with a preferred (D) or null (E) stimuli
662 (bottom, input timing). Color coding as in (B).

663 (F) As for (C) for focal distribution. Shades mark S.D.

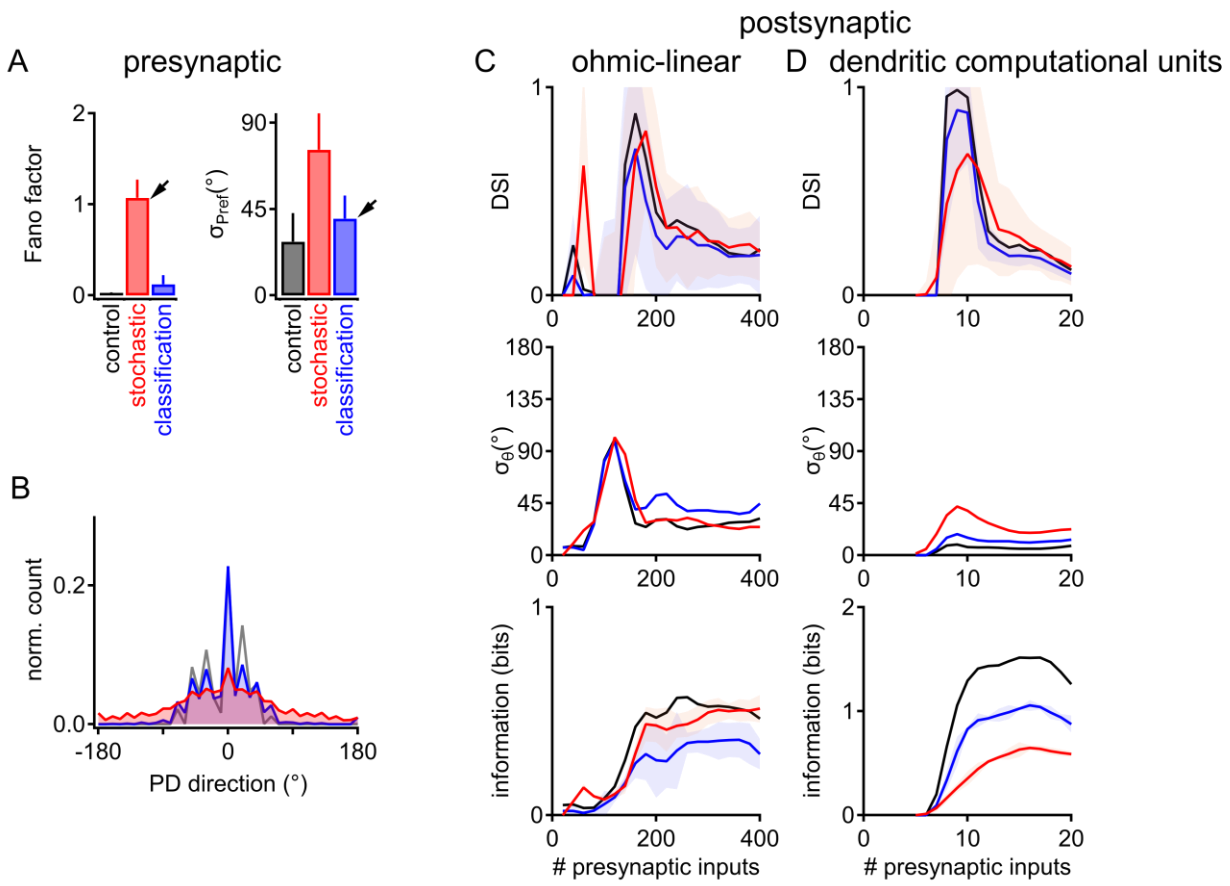

664

665 **Figure 4-figure supplement 1: Computation of direction selectivity in a reconstructed cortical layer**

666 **2/3 pyramidal cell.**

667 (A, B) Variability metrics of the presynaptic input. (A) Left, Fano factor (variance/mean)

668 computed in the absence of noise (black), in the presence of stochastic variability (red, the arrow

669 indicates that this variability level was imposed on the system) and with classification errors

670 (blue). Right, the variability of the angle of the PD computed from the distribution of calculated

671 PDs for 1000 presynaptic cells (B). The distribution in (B) was computed using rounds of 8

672 directionally symmetric stimulation trials. Non-zero variability in noise-free condition reflects

673 differences in directional tuning between different cells.

674 (C, D) Metrics of direction selectivity calculated from the postsynaptic action potentials as a

675 function of the number of synaptic inputs for ohmic-linear (C) and dendritic subunit (D)

676 integration scenarios. n=1000 rounds (8 trials each) for each input intensity. Shades mark S.D.

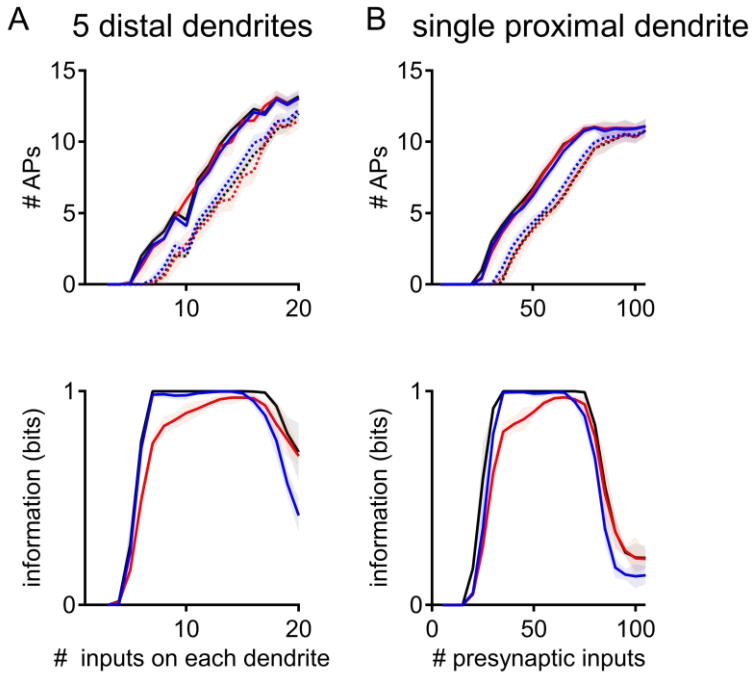

677

678 **Figure 7-figure supplement 1: Synaptic noise tolerance is similar between inputs activated on**

679 **multiple distal branches to the stimulation of a single proximal site in a cortical layer 5 pyramidal**

680 **cell.**

681 The cell was innervated with an increasing number of presynaptic inputs that were either evenly

682 distributed between five distal branches (A) or focused on a single proximal dendrite (A). Top,

683 the number of postsynaptic action potentials for preferred (solid) and null (dotted) stimulations.

684 Bottom, the mutual information derived from the firing output of the cell. n=1000 repeats for

685 each condition, shades mark S.D.

686

687 **References**

688 Babadi, B., and Sompolinsky, H. (2014). Sparseness and expansion in sensory representations. Neuron
689 83, 1213-1226.
690 Beck, J.M., Ma, W.J., Pitkow, X., Latham, P.E., and Pouget, A. (2012). Not noisy, just wrong: the role of
691 suboptimal inference in behavioral variability. Neuron 74, 30-39.
692 Behabadi, B.F., Polsky, A., Jadi, M., Schiller, J., and Mel, B.W. (2012). Location-dependent excitatory
693 synaptic interactions in pyramidal neuron dendrites. PLoS computational biology 8, e1002599.
694 Benucci, A., Saleem, A.B., and Carandini, M. (2013). Adaptation maintains population homeostasis in
695 primary visual cortex. Nat Neurosci 16, 724-729.
696 Branco, T., and Hausser, M. (2010). The single dendritic branch as a fundamental functional unit in the
697 nervous system. Current opinion in neurobiology 20, 494-502.
698 Branco, T., and Hausser, M. (2011). Synaptic integration gradients in single cortical pyramidal cell
699 dendrites. Neuron 69, 885-892.
700 Cafaro, J., and Rieke, F. (2010). Noise correlations improve response fidelity and stimulus encoding.
701 Nature 468, 964-967.
702 DeWeese, M.R., Wehr, M., and Zador, A.M. (2003). Binary spiking in auditory cortex. J Neurosci 23,
703 7940-7949.
704 Faisal, A.A., Selen, L.P., and Wolpert, D.M. (2008). Noise in the nervous system. Nat Rev Neurosci 9, 292-
705 303.
706 Fellous, J.M., Rudolph, M., Destexhe, A., and Sejnowski, T.J. (2003). Synaptic background noise controls
707 the input/output characteristics of single cells in an in vitro model of in vivo activity. Neuroscience 122,
708 811-829.
709 Felsen, G., Shen, Y.S., Yao, H., Spor, G., Li, C., and Dan, Y. (2002). Dynamic modification of cortical
710 orientation tuning mediated by recurrent connections. Neuron 36, 945-954.

711 Franke, F., Fiscella, M., Sevelev, M., Roska, B., Hierlemann, A., and da Silveira, R.A. (2016). Structures of
712 Neural Correlation and How They Favor Coding. Neuron 89, 409-422.
713 Gambino, F., Pages, S., Kehayas, V., Baptista, D., Tatti, R., Carleton, A., and Holtmaat, A. (2014). Sensory-
714 evoked LTP driven by dendritic plateau potentials in vivo. Nature 515, 116-119.
715 Gollnick, C.A., Millard, D.C., Ortiz, A.D., Bellamkonda, R.V., and Stanley, G.B. (2016). Response reliability
716 observed with voltage-sensitive dye imaging of cortical layer 2/3: the probability of activation
717 hypothesis. J Neurophysiol 115, 2456-2469.
718 Grienberger, C., Chen, X., and Konnerth, A. (2014). NMDA Receptor-Dependent Multidendrite Ca(2+)
719 Spikes Required for Hippocampal Burst Firing In Vivo. Neuron 81, 1274-1281.
720 Guerguiev, J., Lillicrap, T.P., and Richards, B.A. (2017). Towards deep learning with segregated dendrites.
721 Elife 6.
722 Hausser, M., and Mel, B. (2003). Dendrites: bug or feature? Current opinion in neurobiology 13, 372-
723 383.
724 Hawkins, J., and Ahmad, S. (2016). Why Neurons Have Thousands of Synapses, a Theory of Sequence
725 Memory in Neocortex. Frontiers in neural circuits 10, 23.
726 Hires, S.A., Gutnisky, D.A., Yu, J., O'Connor, D.H., and Svoboda, K. (2015). Low-noise encoding of active
727 touch by layer 4 in the somatosensory cortex. Elife 4.
728 Jeyabalaratnam, J., Bharmauria, V., Bachatene, L., Cattan, S., Angers, A., and Molotchnikoff, S. (2013).
729 Adaptation shifts preferred orientation of tuning curve in the mouse visual cortex. PLoS One 8, e64294.
730 Jia, H., Rochefort, N.L., Chen, X., and Konnerth, A. (2010). Dendritic organization of sensory input to
731 cortical neurons in vivo. Nature 464, 1307-1312.
732 Kaifosh, P., and Losonczy, A. (2016). Mnemonic Functions for Nonlinear Dendritic Integration in
733 Hippocampal Pyramidal Circuits. Neuron 90, 622-634.

734 Kohn, A., Coen-Cagli, R., Kanitscheider, I., and Pouget, A. (2016). Correlations and Neuronal Population
735 Information. Annu Rev Neurosci 39, 237-256.
736 Lavzin, M., Rapoport, S., Polsky, A., Garion, L., and Schiller, J. (2012). Nonlinear dendritic processing
737 determines angular tuning of barrel cortex neurons in vivo. Nature 490, 397-401.
738 London, M., and Hausser, M. (2005). Dendritic computation. Annual review of neuroscience 28, 503-
739 532.
740 London, M., Roth, A., Beeren, L., Hausser, M., and Latham, P.E. (2010). Sensitivity to perturbations in
741 vivo implies high noise and suggests rate coding in cortex. Nature 466, 123-127.
742 Magee, J.C. (2000). Dendritic integration of excitatory synaptic input. Nature reviews Neuroscience 1,
743 181-190.
744 Major, G., Larkum, M.E., and Schiller, J. (2013). Active properties of neocortical pyramidal neuron
745 dendrites. Annual review of neuroscience 36, 1-24.
746 Major, G., Polsky, A., Denk, W., Schiller, J., and Tank, D.W. (2008). Spatiotemporally graded NMDA
747 spike/plateau potentials in basal dendrites of neocortical pyramidal neurons. Journal of neurophysiology
748 99, 2584-2601.
749 Manita, S., Miyakawa, H., Kitamura, K., and Murayama, M. (2017). Dendritic Spikes in Sensory
750 Perception. Front Cell Neurosci 11, 29.
751 McCulloch, W.S., and Pitts, W. (1990). A logical calculus of the ideas immanent in nervous activity. 1943.
752 Bulletin of mathematical biology 52, 99-115; discussion 173-197.
753 Oesch, N., Euler, T., and Taylor, W.R. (2005). Direction-selective dendritic action potentials in rabbit
754 retina. Neuron 47, 739-750.
755 Palmer, L.M., Shai, A.S., Reeve, J.E., Anderson, H.L., Paulsen, O., and Larkum, M.E. (2014). NMDA spikes
756 enhance action potential generation during sensory input. Nature neuroscience 17, 383-390.

757 Petersen, C.C.H. (2017). Whole-Cell Recording of Neuronal Membrane Potential during Behavior.
758 Neuron 95, 1266-1281.
759 Poirazi, P., Brannon, T., and Mel, B.W. (2003). Pyramidal neuron as two-layer neural network. Neuron
760 37, 989-999.
761 Poleg-Polsky, A., Ding, H., and Diamond, J.S. (2018). Functional Compartmentalization within Starburst
762 Amacrine Cell Dendrites in the Retina. Cell reports 22, 2898-2908.
763 Polsky, A., Mel, B., and Schiller, J. (2009). Encoding and decoding bursts by NMDA spikes in basal
764 dendrites of layer 5 pyramidal neurons. The Journal of neuroscience : the official journal of the Society
765 for Neuroscience 29, 11891-11903.
766 Polsky, A., Mel, B.W., and Schiller, J. (2004). Computational subunits in thin dendrites of pyramidal cells.
767 Nature neuroscience 7, 621-627.
768 Ranjbar-Slamloo, Y., and Arabzadeh, E. (2017). High-velocity stimulation evokes "dense" population
769 response in layer 2/3 vibrissal cortex. J Neurophysiol 117, 1218-1228.
770 Rhodes, P.A. (2008). Recoding patterns of sensory input: higher-order features and the function of
771 nonlinear dendritic trees. Neural computation 20, 2000-2036.
772 Rivlin-Etzion, M., Wei, W., and Feller, M.B. (2012). Visual stimulation reverses the directional preference
773 of direction-selective retinal ganglion cells. Neuron 76, 518-525.
774 Schiess, M., Urbanczik, R., and Senn, W. (2016). Somato-dendritic Synaptic Plasticity and Error-
775 backpropagation in Active Dendrites. PLoS computational biology 12, e1004638.
776 Schiller, J., Major, G., Koester, H.J., and Schiller, Y. (2000). NMDA spikes in basal dendrites of cortical
777 pyramidal neurons. Nature 404, 285-289.
778 Schmidt-Hieber, C., Toleikyte, G., Aitchison, L., Roth, A., Clark, B.A., Branco, T., and Hausser, M. (2017).
779 Active dendritic integration as a mechanism for robust and precise grid cell firing. Nature neuroscience
780 20, 1114-1121.

781 Shannon, C.E. (1948). A Mathematical Theory of Communication. Bell System Technical Journal 27, 379-
782 423.
783 Sheffield, M.E., and Dombeck, D.A. (2015). Calcium transient prevalence across the dendritic arbour
784 predicts place field properties. Nature 517, 200-204.
785 Sivyer, B., and Williams, S.R. (2013). Direction selectivity is computed by active dendritic integration in
786 retinal ganglion cells. Nature neuroscience 16, 1848-1856.
787 Smith, S.L., Smith, I.T., Branco, T., and Hausser, M. (2013). Dendritic spikes enhance stimulus selectivity
788 in cortical neurons in vivo. Nature 503, 115-120.
789 Spencer, W.A., and Kandel, E.R. (1961). Electrophysiology of Hippocampal Neurons: Iv. Fast
790 Prepotentials. Journal of neurophysiology 24, 272-285.
791 Sun, W., Tan, Z., Mensh, B.D., and Ji, N. (2016). Thalamus provides layer 4 of primary visual cortex with
792 orientation- and direction-tuned inputs. Nature neuroscience 19, 308-315.
793 Takahashi, N., Oertner, T.G., Hegemann, P., and Larkum, M.E. (2016). Active cortical dendrites modulate
794 perception. Science 354, 1587-1590.
795 Tao, C., Zhang, G., Zhou, C., Wang, L., Yan, S., Zhang, L.I., Zhou, Y., and Xiong, Y. (2016). Synaptic Basis for
796 the Generation of Response Variation in Auditory Cortex. Sci Rep 6, 31024.
797 Trenholm, S., McLaughlin, A.J., Schwab, D.J., Turner, M.H., Smith, R.G., Rieke, F., and Awatramani, G.B.
798 (2014). Nonlinear dendritic integration of electrical and chemical synaptic inputs drives fine-scale
799 correlations. Nature neuroscience 17, 1759-1766.
800 Wilson, D.E., Whitney, D.E., Scholl, B., and Fitzpatrick, D. (2016). Orientation selectivity and the
801 functional clustering of synaptic inputs in primary visual cortex. Nat Neurosci 19, 1003-1009.
802 Wu, X.E., and Mel, B.W. (2009). Capacity-enhancing synaptic learning rules in a medial temporal lobe
803 online learning model. Neuron 62, 31-41.

804 Zavitz, E., Yu, H.H., Rosa, M.G.P., and Price, N.S.C. (2017). Correlated Variability in the Neurons With the
805 Strongest Tuning Improves Direction Coding. Cereb Cortex.
806 Zhu, Y., Qiao, W., Liu, K., Zhong, H., and Yao, H. (2015). Control of response reliability by parvalbumin-
807 expressing interneurons in visual cortex. Nat Commun 6, 6802.
808 Zylberberg, J., Cafaro, J., Turner, M.H., Shea-Brown, E., and Rieke, F. (2016). Direction-Selective Circuits
809 Shape Noise to Ensure a Precise Population Code. Neuron 89, 369-383.
810 Zylberberg, J., Pouget, A., Latham, P.E., and Shea-Brown, E. (2017). Robust information propagation
811 through noisy neural circuits. PLoS Comput Biol 13, e1005497.

812